ORIGINAL PAPER

Effect of Volatile Species on Chemical Vapour Deposition of SiO$_2$ During Corrosion of Chromia- and Alumina-Formers

Thuan Dinh Nguyen[1] · Jianqiang Zhang[1] · David J. Young[1]

Abstract

Silicon-bearing vapour at low pressure was used to deposit SiO$_2$ during exposure of pure chromium, Fe-30Cr (wt.%) and Kanthal APM alloy to an Ar-10H$_2$O-0.1HCl mixture (vol.%) at 650 °C. Pure Cr formed porous chromia blades on top of a poly-crystalline Cr$_2$O$_3$ scale containing SiO$_2$. A model Fe-30Cr alloy formed a scale consisting of a thick, amorphous (Cr,Si)O$_x$ outer layer and a thin, polycrystalline Cr$_2$O$_3$ inner layer. Kanthal alloy formed a thin scale containing a Si-rich oxide outer layer and an inner layer of Fe, Cr, and Al oxides. Amorphous (Cr,Si)O$_x$ nodules formed locally on top of (Cr,Fe)$_{23}$C$_6$ precipitates at the Kanthal surface.

Introduction

The amount of waste generated by economic activity and population growth is a major concern for human health and the environment. Burning waste to generate energy is a sustainable solution to reduce mounting volumes of landfill. However, burning waste may release highly corrosive gases that can degrade steels used in heat exchangers. Products containing polyvinyl chloride (PVC) and silicone are widely used in industries and daily life. For this reason, waste combustion usually produces a flue gas containing HCl, H$_2$O, and volatile Si species as well as CO$_2$.

The high temperature corrosion resistance of common heat-resistant alloys relies on their ability to form and maintain a dense, slow-growing scale of Cr$_2$O$_3$ or Al$_2$O$_3$. These oxide scales are usually polycrystalline. Surprisingly, corrosion of Fe-30Cr in a gas mixture of H$_2$O, HCl, and siloxane at 650 °C has been found to form a duplex

✉ Jianqiang Zhang
 j.q.zhang@unsw.edu.au

1 School of Materials Science and Engineering, University of New South Wales, Sydney, NSW 2052, Australia

scale, consisting of an outer, amorphous $(Cr,Si)O_x$ layer and a thinner, inner polycrystalline Cr_2O_3 layer [1]. The $(Cr,Si)O_x$ compound contains Cr (30–41 at.%), Si (7–11 at.%), Fe (~1 at.%), and oxygen (balance). It was suggested [1] that the formation of amorphous $(Cr,Si)O_x$ is controlled by vaporisation and oxidation of volatile species of both Cr and Si species.

Because the novel amorphous $(Cr,Si)O_x$ scale cannot provide grain boundary transport, it may provide a better corrosion barrier than a normal polycrystalline Cr_2O_3 scale, and $(Cr,Si)O_x$ might itself grow slower than Cr_2O_3. A better understanding of the growth mechanism of amorphous $(Cr,Si)O_x$ potentially offers a route to a new coating design for high temperature corrosion applications. It is therefore important to know how widespread the phenomenon is: does it depend on the alloy base metal; does it extend to alumina-forming alloys?

In this paper, chemical vapour deposition of SiO_2 onto pure chromium was compared with that of Fe-30Cr during exposure to Ar-10H_2O-0.1HCl at 650 °C, with the aim of revealing any effects of Fe species on the formation of amorphous $(Cr,Si)O_x$. Kanthal alloy was also selected as it usually forms a protective Al_2O_3 scale, and its effect on the formation of amorphous Si-bearing oxide was also investigated.

Experimental Procedures

Pure Cr metal and two alloys, a model Fe-30Cr (wt.%) and commercial Kanthal APM were used for the experiments. The pure Cr and Fe-30Cr were prepared by arc melting pure metals Cr (99.995%, Sigma Aldrich) and Fe (99.98%, Sigma Aldrich) under a protective Ar-5%H_2 (volume %) gas atmosphere, using a non-consumable electrode. The resulting Fe-30Cr button was annealed at 1000 °C for 70 h in a flowing Ar-5%H_2 gas for homogenization. Rectangular sample coupons (1.1–2.3)×(8.1–10.4)×(4–8.8) mm³ in size were surface ground to a 1200-grit finish and ultrasonically cleaned in ethanol prior to reaction. The Fe-30Cr alloy composition was checked by SEM/EDX (detection limit of 0.1 wt. %) and found to be Fe-(29.8±0.1)Cr (wt.%). An Inductively Coupled Plasma (ICP) analysis revealed the Fe-30Cr alloy to contain about 0.002 wt.% Si as an impurity. The Kanthal APM alloy composition in Table 1 was analysed by ICP-AES.

All specimens were reacted at 650 °C in Ar-10H_2O-0.1HCl mixture (volume %) with a linear flow rate of 1 cm/s and a total pressure of 1 atm for up to 240 h. The equilibrium partial pressures of minority species in Ar-10H_2O-0.1HCl are shown in Table 2. A horizontal alumina tube furnace was used, and the experimental setup is shown in the previous study [1]. Argon was flowed at controlled rates through a flask containing HCl solution at a controlled temperature, yielding the desired partial pressures of H_2O and HCl [2]. The flask was refilled frequently with HCl solution during experiments. Concentrated hydrochloric acid (RCI Labscan) was diluted with

Table 1 Composition of commercial Kanthal APM alloy (wt. %) by ICP-AES

Fe	Cr	Al	Si	Mn	P	Ni	Mo	Ti	C
Bal	21.8	5.95	0.33	0.17	0.02	0.22	0.02	0.05	0.03

Table 2 Equilibrium gas composition of Ar-10H$_2$O-0.1HCl at 650 °C calculated by Factsage [4]

	Species		
	O$_2$	H$_2$	Cl$_2$
Pressure (atm)	4.5×10^{-9}	1.1×10^{-8}	4.1×10^{-10}

deionized water to make a 15.5% HCl (wt. %) solution for the required H$_2$O + HCl gas mixtures. Heating tapes were used to prevent condensation inside the glass tubes connecting the condenser to the reactor tube's end cap and set at 88 °C. The exhaust gas was scrubbed through KOH solution to absorb the remaining HCl.

No silicone grease was used at glassware joints to avoid potential Si contamination from this source. Silicone oil (Polydimethylsiloxane, Rhodorsil oil 47 V 350, Bluestar Silicones) was placed in an alumina crucible near the reactor inlet cap [1], and an Ar-10H$_2$O-0.1HCl gas mixture flowed over it into the heated reactor tube. Alloy samples were suspended in an alumina crucible using Kanthal alloy wire.

Weight changes of corroded samples were measured using an analytic balance (Mettler Toledo) with an accuracy of 0.01 mg. Corroded samples were characterized by scanning electron microscopy (SEM, Hitachi S3400) with an energy dispersive X-ray spectrometer (EDX, Bruker) and transmission electron microscopy (TEM, JEOL JEM-F200). The TEM samples were prepared using a focused ion beam system (FIB, FEI Nova Nanolab 200) with a maximum accelerating voltage of 30 kV.

Results

Weight gain kinetics of Cr, Fe-30Cr, and Kanthal are shown in Fig. 1. Weight uptakes increased slowly with time, Kanthal exhibiting the smallest weight uptakes. No scale spallation was observed during cooling.

Reaction Products on Chromium

Surface morphologies of the reaction product on pure Cr after exposure for 20 and 240 h are shown in Fig. 2. Porous oxide blades formed on the sample surface and grew with time. Fine oxide grains were observed randomly located on the oxide blade surfaces after the 240 h reaction (Fig. 2b).

A cross-sectional bright field-scanning transmission electron microscopy (BF-STEM) image of pure Cr corroded for 20 h is shown in Fig. 3a. Analyses by EDX (Fig. 3b, d, e) and SAD pattern (Fig. 3c) revealed that the Cr$_2$O$_3$ blades formed on top of a solid, duplex Cr$_2$O$_3$ layer consisting of an outer, Si-rich layer (layer X, 160 ± 60 nm) and an inner layer (layer Y, 360 ± 100 nm). Silicon contents were high in the outer layer (2.9–8.3 at.% Si) but lower in the inner layer (0.3–0.4 at.% Si) (Fig. 3a, d, e). The outer layer contained fine oxide grains whilst a mixture of fine

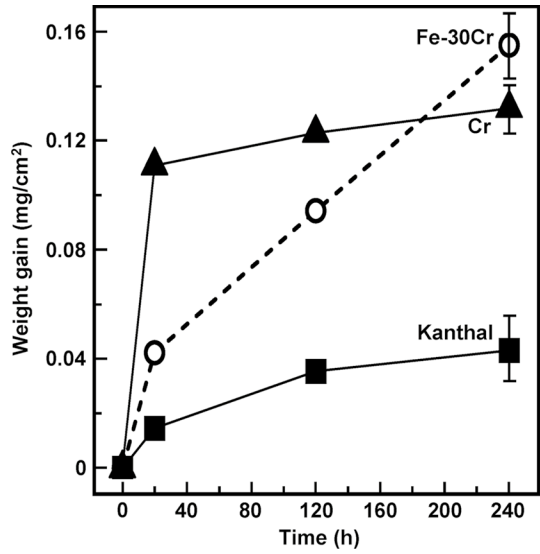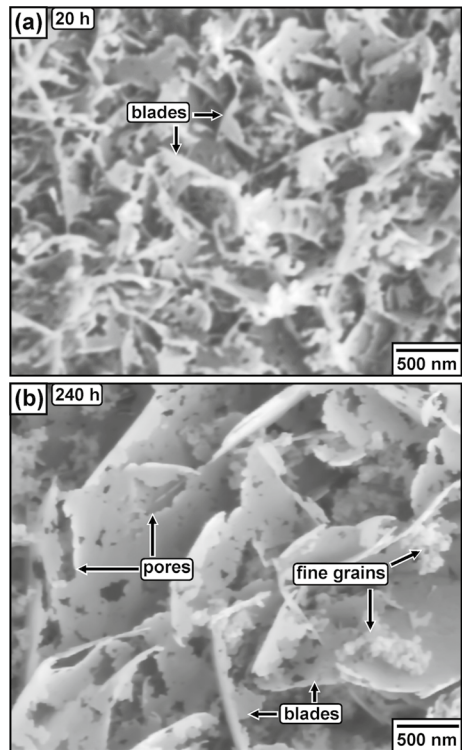**Fig. 1** Weight gain kinetics of pure Cr, Fe-30Cr, and Kanthal alloy

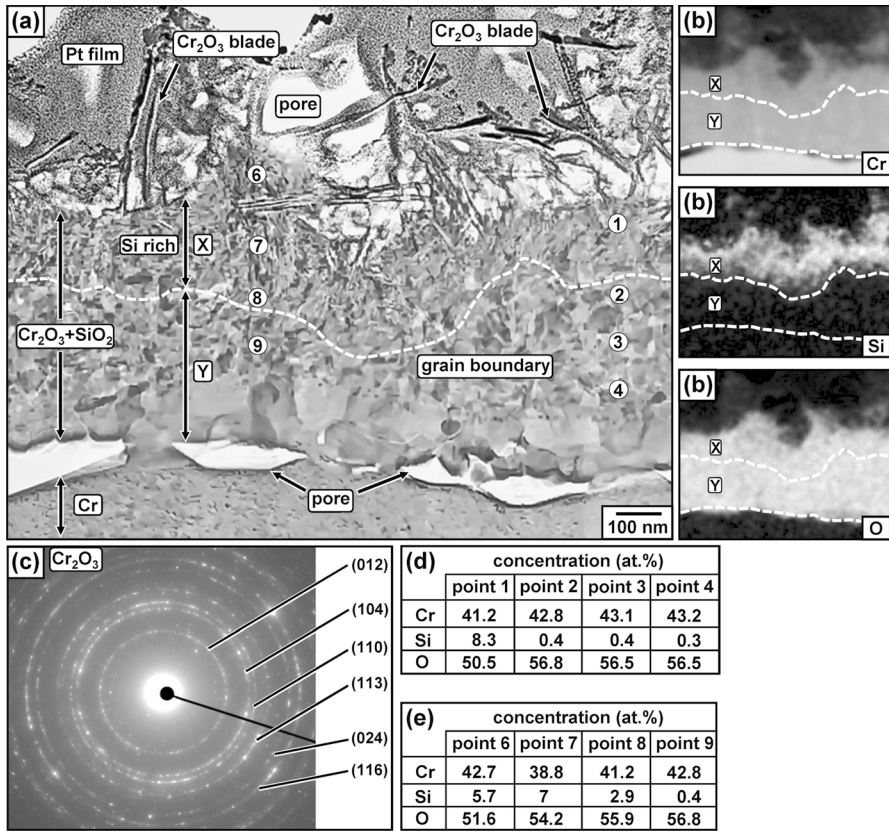**Fig. 2** SE-SEM top view of pure Cr reacted for **a** 20 h and **b** 240 h

(d)	concentration (at.%)			
	point 1	point 2	point 3	point 4
Cr	41.2	42.8	43.1	43.2
Si	8.3	0.4	0.4	0.3
O	50.5	56.8	56.5	56.5

(e)	concentration (at.%)			
	point 6	point 7	point 8	point 9
Cr	42.7	38.8	41.2	42.8
Si	5.7	7	2.9	0.4
O	51.6	54.2	55.9	56.8

Fig. 3 Pure Cr corroded for 20 h: **a** BF-STEM cross-section, **b** EDX mapping, and **c** SAD pattern of the whole scale in (**a**), and EDX concentrations of **d** points1-5 and **e** points 6–9 in (**a**)

and coarse grains made up the inner layer (Fig. 3a). Chromia was identified by SAD, but no crystalline silica phases were detected.

When the reaction continued to 240 h (Fig. 4), pure Cr formed the same oxidation products. Silicon was found in the outer layer (5.1–9.5 at.% Si) and inner layer (0.2–0.9 at.% Si) (Fig. 4a, d, e). The outer layer (220 ± 60 nm) contained only fine grains (Fig. 4f, g), but coarse grains were mainly observed in the inner layer (about 135 ± 50 nm). The Si concentration in the scale was significant but only crystalline Cr_2O_3 was detected from the SAD pattern (Fig. 4c), indicating SiO_2 to be amorphous if present. The high magnification images (Fig. 4f, g) further confirmed the outer layer to be polycrystalline.

Reaction Products on Fe-30Cr

The scale on Fe-30Cr was found by TEM/EDX analysis to consist of an outer (Cr,Si) O_x layer (about 330 nm) and an inner, polycrystalline Cr_2O_3 layer (about 50 nm)
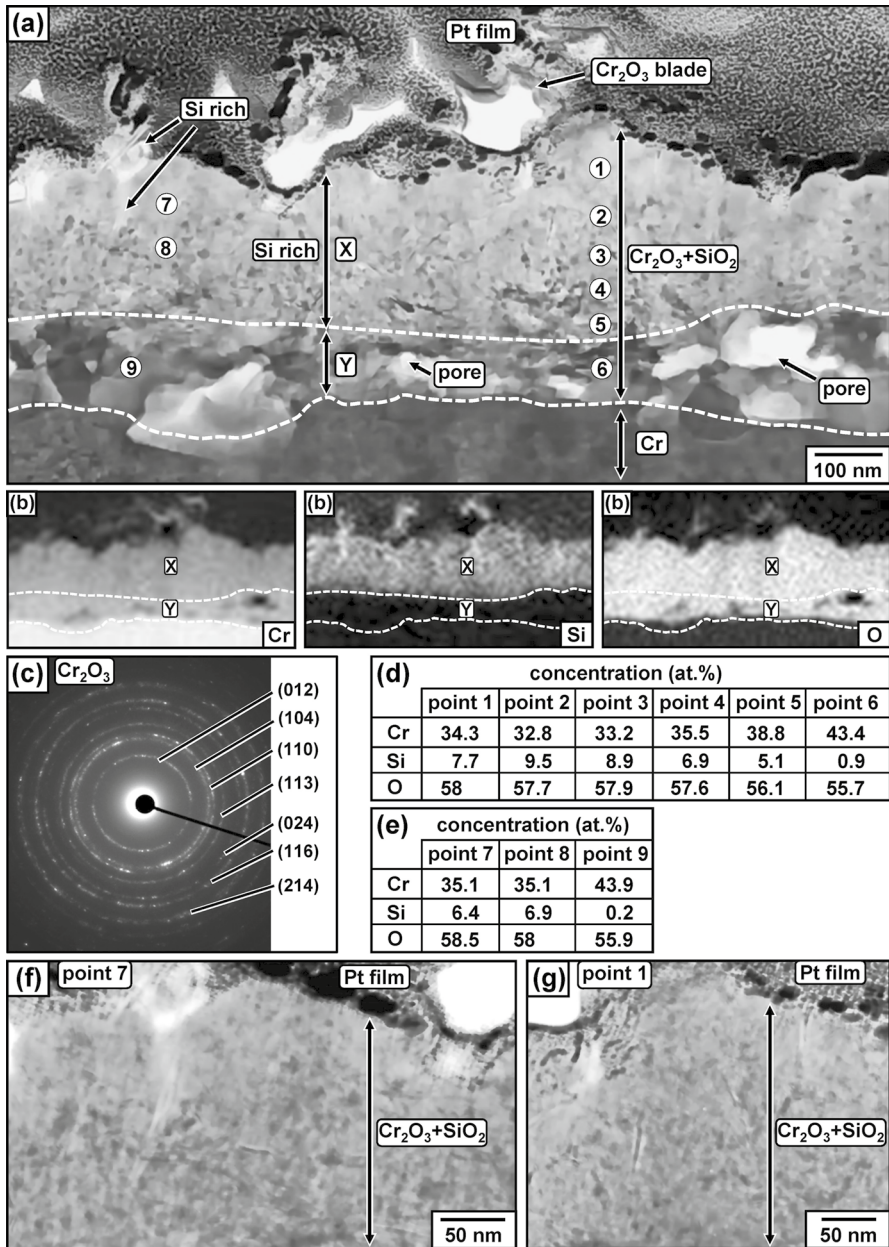
Fig. 4 Pure Cr corroded for 240 h: **a** BF-STEM cross-section, **b** EDX mapping, and **c** SAD pattern of the outer scale layer in (**a**), EDX concentrations of **d** points1-6 and **e** points 7–9 in (**a**), and high magnification images of areas around **f** point 7 and **g** point 1 in (**a**)
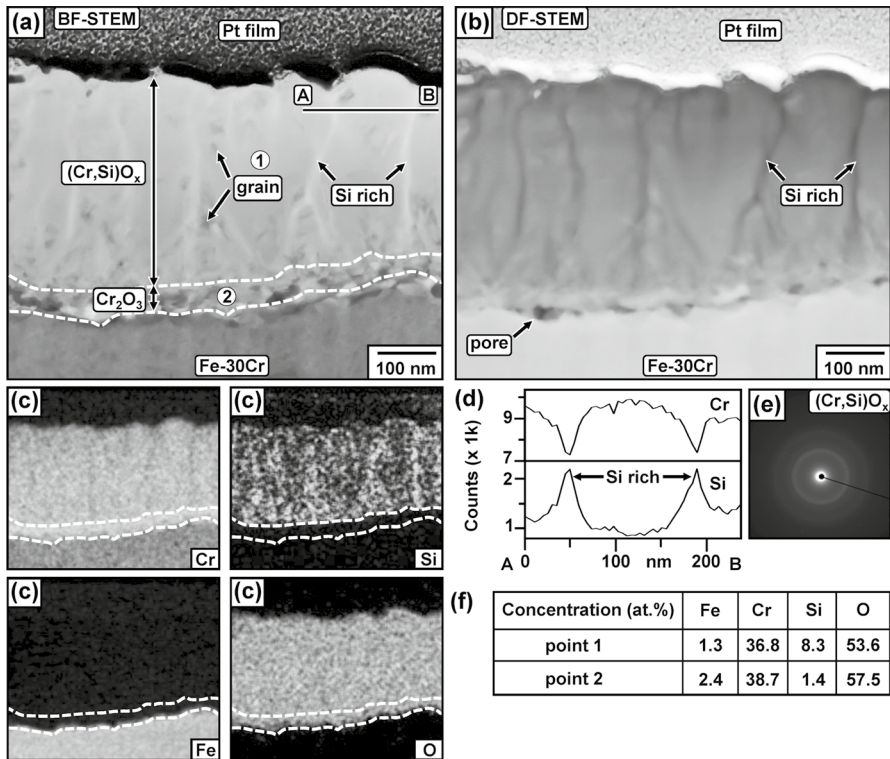
Fig. 5 Fe-30Cr corroded for 240 h: **a** BF-STEM and **b** DF-STEM cross-sections, **c** EDX mapping, **d** EDX line profiles along A-B in (**a**), **e** SAD pattern at point 1 in (**a**), and **f** EDX concentrations of points 1–2 in (**a**)

(Fig. 5a, c, f). The $(Cr,Si)O_x$ layer contained about 8.3 at.% Si, and about 1.4 at.% Si was found in the Cr_2O_3 layer (Fig. 5a, f). A selected area diffraction pattern (SAD) at point 1(Fig. 5a, e) shows the $(Cr,Si)O_x$ layer to be amorphous, but fine crystalline grains [1] were still observed distributed randomly in this layer (Fig. 5a). Silicon-rich veins in the $(Cr,Si)O_x$ layer had a bright contrast in the BF-STEM image (Fig. 5a, d) and were visible by their dark contrast in the DF-STEM (Fig. 5b).

Reaction Products on Kanthal

The Kanthal alloy corroded for 240 h was covered by a thin scale, with dark and bright SE contrast regions (Fig. 6a). A high magnification image (Fig. 6b) and SEM/EDX mapping (Fig. 6c) indicate the bright contrast regions (surface area fraction of 33%) to be rich in Si and the dark contrast regions rich in Al. The scale surface of the Al-rich region (Fig. 6e) was smoother than that of the Si-rich region, which contained fine oxide blades (Fig. 6d). The small nodules visible in Figs. 6b, f were found by SEM/EDX (Fig. 6g) to be granular in appearance (Fig. 6h) and rich in both Cr and Si.
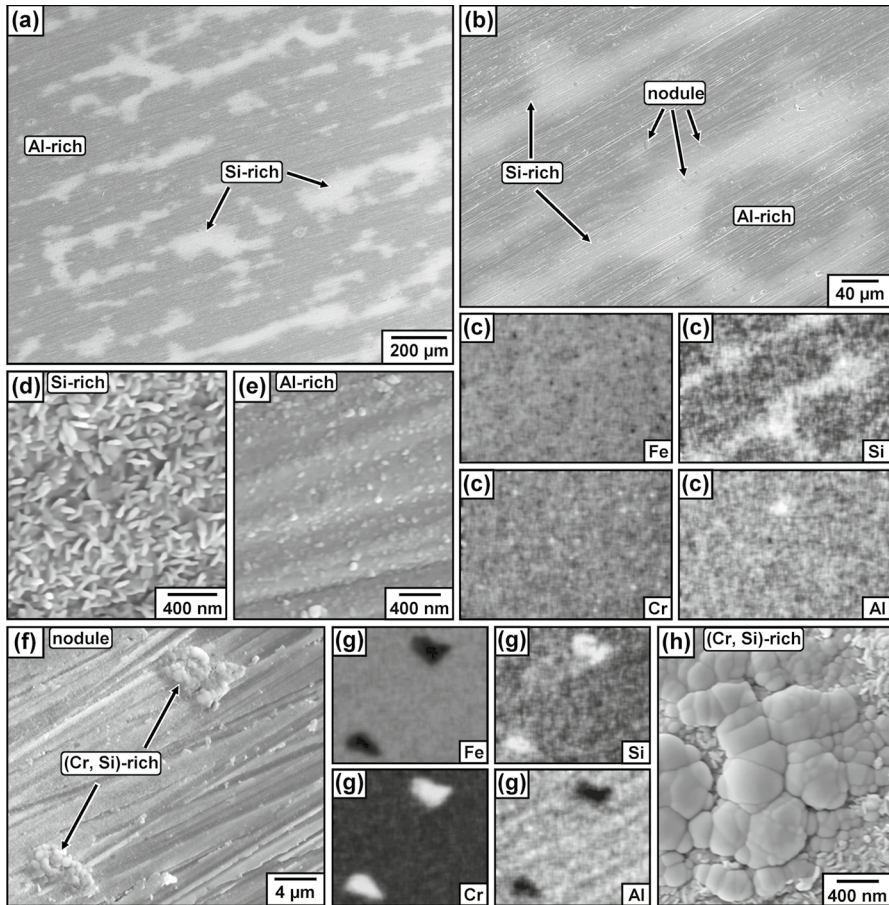
Fig. 6 Kanthal alloy corroded for 240 h: **a** SE-SEM top view, **b** high magnification image of (**a**), **c** EDX mapping of (**b**), high magnification images of **d** Si-rich and **e** Al-rich regions in (**b**), **f** enlarged image of nodules in (**b**), **g** EDX mapping of (**f**), and **h** high magnification image of (Cr, Si)-rich nodules

A BF-STEM cross-section of the (Cr, Si)-rich nodule in Fig. 6f formed on Kanthal after 240 h reaction is shown in Fig. 7a. A dark contrast grain beneath the (Cr, Si)-rich nodule (Fig. 7a) was analysed by EDX (Fig. 7b, c) and a SAD pattern (Fig. 7d) confirmed it to be $(Cr,Fe)_{23}C_6$. A spectrum of the $(Cr,Fe)_{23}C_6$ grain in Fig. 7c shows a small Al peak, with a ratio of Cr:Fe:Al (at.%) = 52.5:14.8:0.2.

Analyses by EDX (Fig. 7g, k) and a SAD pattern (Fig. 7e) revealed that the (Cr, Si)-rich nodule (Fig. 7f, h) was made of an outer, amorphous $(Cr,Si)O_x$ region (about 310 nm, 8.5–18.9 at.% Si), an intermediate Cr-rich oxide layer, and an inner Al_2O_3 layer (about 16 nm). Enrichment of Fe was observed locally beneath the nodule-carbide interface (Fig. 7f, g, h). A Si-rich vein had a dark contrast in the DF-STEM image (Fig. 7h, m) and a white contrast in the BF-STEM (Fig. 7f),
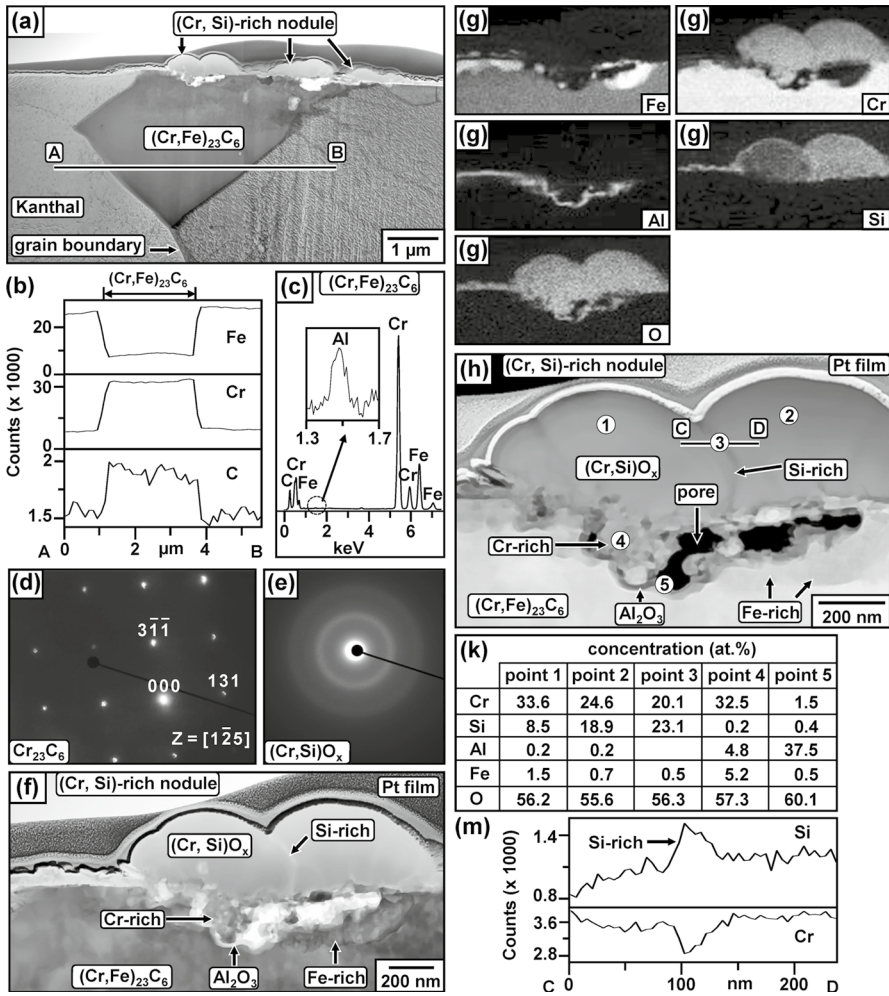
Fig. 7 Kanthal alloy corroded for 240 h: **a** BF-STEM cross-section of (Cr, Si)-rich nodule in Fig. 6f, **b** EDX line profiles along A-B in (**a**), **c** EDS spectrum and **d** SAD pattern of $(Cr,Fe)_{23}C_6$ particle in (**a**), **e** SAD pattern of $(Cr,Si)O_x$ in (**f**), **f** high magnification image of (**a**), **g** EDX mapping of (**f**), **h** enlarged DF-STEM image of the (Cr, Si)-rich nodule in (**f**), **k** EDX concentrations of points1-5 in (**h**), and **m** EDX line profiles along C-D in (**h**)

containing about 23.1 at.% Si (point 3 in Fig. 7h, k). A thin Al-rich oxide scale is seen in Fig. 7f, g to cover the alloy surface surrounding the nodule, and a similar layer had developed at the nodule-alloy interface.

A BF-TEM cross-section of the Si-rich scale region on Kanthal alloy (Fig. 6b) is shown in Fig. 8a. Analysis by EDX (Fig. 8a, b, c) revealed that the scale consisted of an outer, (Si, Fe)-rich layer (50 ± 20 nm) and an inner, (Al, Cr)-rich layer (42 ± 8 nm). The outer layer contained dark contrast, Fe-rich
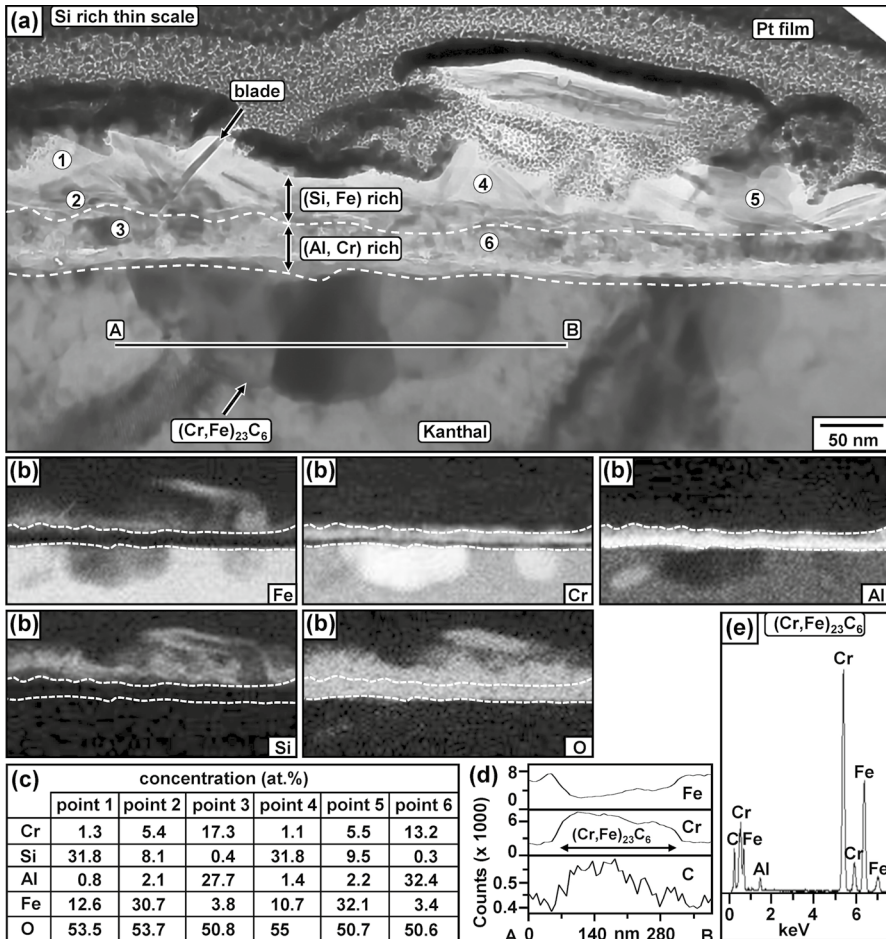
Fig. 8 Kanthal alloy corroded for 240 h: **a** BF-TEM cross-section of Si-rich thin scale in Fig. 6d, **b** EDX mapping, **c** EDX concentrations of points1-6 in (**a**), **d** EDX line profiles along A-B and **e** EDS spectrum of $(Cr,Fe)_{23}C_6$ particles in (**a**)

blades/grains covered by a bright contrast Si-rich layer (about 31.8 at.% Si). Carbide precipitates were observed beneath the scale, with a ratio of Cr:Fe:Al (at.%) = 40.6:17.4:1.8 (Fig. 8a, b, d, e).

The Al-rich scale region on Kanthal alloy reacted for 240 h (Fig. 6e) was analysed by TEM/EDX and found to consist of an outer, Si-rich oxide layer (15 ± 3 nm) and an inner, (Al, Cr) rich layer (27 ± 3 nm) (Fig. 9a, b). The Si concentrations are about 28.6 at.% in the outer layer and 3.1 at.% in the (Al, Cr)-rich layer.

The phase diagram calculated by Thermocalc [3] in Fig. 10 predicted the Kanthal alloy to form $M_{23}C_6$ carbide.

Fig. 9 Kanthal alloy corroded for 240 h: **a** BF-STEM cross-section of Al-rich thin scale in Fig. 6e, **b** EDX line profiles along A-B, and **c** EDX concentrations of points 1-2 in (**a**)
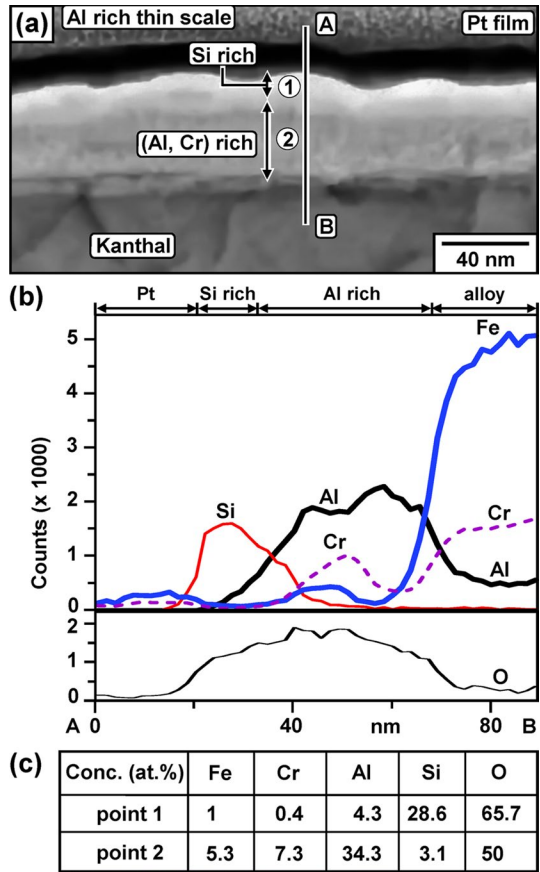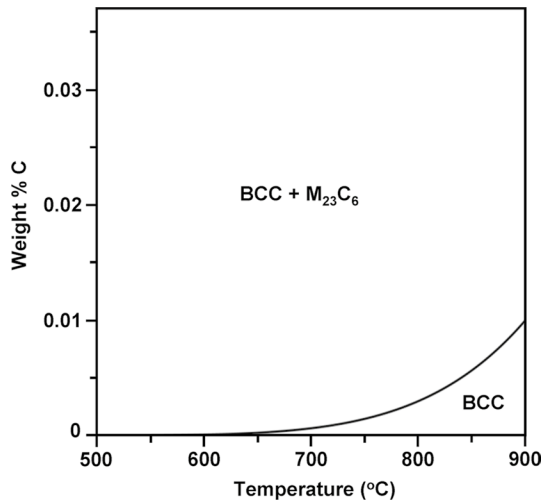

Conc. (at.%)	Fe	Cr	Al	Si	O
point 1	1	0.4	4.3	28.6	65.7
point 2	5.3	7.3	34.3	3.1	50

Fig. 10 Phase diagram of the Fe-21.8Cr-5.95Al-0.33Si-0.17Mn-0.22Ni-0.03C system calculated by Thermocalc

Discussion

The formation of Si-containing scales on pure Cr, Fe-30Cr, and Kanthal confirmed formation of volatile Si species and deposition onto each metal surface. A new amorphous $(Cr,Si)O_x$ phase was observed over the whole surface of Fe-30Cr and as nodules on Kanthal APM. Chemical vapour deposition (CVD) of SiO_2 is now considered.

CVD of SiO_2 on Pure Cr

Reactions in Ar-10H_2O-0.1HCl-silicone oil gas can result in both vaporisation and oxidation. Oxidation of pure Cr formed a Cr_2O_3 scale.

$$2Cr(s) + 3H_2O(g) = Cr_2O_3(s) + 3H_2(g) \quad \Delta G° = -295.5 \text{ (kJ) [4]} \quad (1)$$
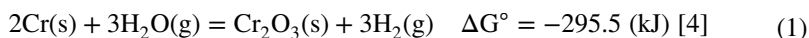
At the scale-metal interface where the oxygen partial pressure was low, vaporisation of Cr is possible at 650 °C if Cl_2 can penetrate the scale.

$$Cr(s) + Cl_2(g) = CrCl_2(g) \quad \Delta G° = -183.9 \text{ (kJ) [4]} \quad (2)$$
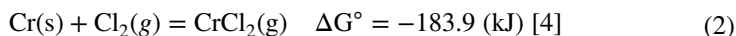
$$p_{CrCl_2} = K_2 a_{Cr} p_{Cl_2} \quad (3)$$

The maximum possible p_{CrCl_2} calculated using activity of Cr ($a_{Cr} = 1$) and partial pressure of Cl_2 ($p_{Cl_2} = 4.1 \times 10^{-10}$ atm) calculated for Ar-10H_2O-0.1HCl at 650 °C is more than 1 atm, revealing that volatile $CrCl_2$ can in principle be formed at the scale-metal interface.

Porous Cr_2O_3 blades were observed on pure Cr after the 240 h reaction, with random clusters of fine grains on the top surface (Fig. 2b). Solid-state diffusion of Cr from the underlying metal to the scale surface is slow and as a result thin, dense Cr_2O_3 scales usually form. In the present case however, superficial porous chromia blades had poor contact with the underlying solid scale after the 20 h reaction (Fig. 2a), but nonetheless continued to grow. When the reaction time increased to 240 h, the blades and pores grew still coarser (Fig. 2b), revealing another Cr supply mechanism available for the blades' growth. It is therefore suggested that the formation of porous blades and clusters of fine grains on top was mainly due to oxidation of volatile Cr chlorides.

$$2CrCl_2(g) + 3/2O_2(g) = Cr_2O_3(s) + 2Cl_2(g) \quad \Delta G° = -518.5 \text{ (kJ) [4]} \quad (4)$$

Pure Cr formed a duplex Cr_2O_3 scale, with the outer layer rich in Si. The inner scale layer got thinner with increasing reaction time: 360 ± 100 nm (20 h, Fig. 3a) and 135 ± 50 nm (240 h, Fig. 4a). Vaporisation of the Cr_2O_3 layer ($a_{Cr_2O_3} = 1$) depends on the equilibrium.

$$Cr_2O_3(s) + 3H_2(g) + 2Cl_2(g) = 2CrCl_2(g) + 3H_2O(g) \quad \Delta G° = -72.2 \text{ (kJ) [4]}$$
$$(5)$$
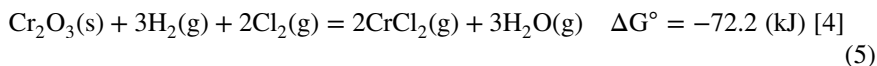
$$p_{CrCl_2} = \left(\frac{K_5 p_{H_2}^3 p_{Cl_2}^2}{p_{H_2O}^3} \right)^{1/2} \tag{6}$$

The p_{CrCl_2} value calculated using partial pressures $p_{Cl_2} = 4.1 \times 10^{-10}$ atm, $p_{H_2} = 1.1 \times 10^{-8}$ atm, and $p_{H_2O} = 0.1$ atm of Ar-10H$_2$O-0.1HCl (Table 2) is 1.7×10^{-18} atm. It is clear that vaporisation of Cr$_2$O$_3$ is negligible on the scale surface and in the outer layer where p_{H_2O} is still significant. At the scale-Cr interface, p_{H_2O} is set by the interfacial equilibrium of reaction (1)

$$K_1 = \frac{p_{H_2}^3}{p_{H_2O}^3} \tag{7}$$

Substitute (7) to (6):

$$p_{CrCl_2} = \left(K_1 K_5 p_{Cl_2}^2 \right)^{1/2} \tag{8}$$

The maximum possible p_{CrCl_2} calculated using $p_{Cl_2} = 4.1 \times 10^{-10}$ atm of Ar-10H$_2$O-0.1HCl at 650 °C is more than 1 atm, indicating that vaporisation of solid Cr$_2$O$_3$ at the scale-metal interface is possible. For this reason, the inner Cr$_2$O$_3$ layer became thinner and developed interfacial pores locally (Fig. 4a) as the reaction time increased.

Silicone oil is polydimethylsiloxane (PDMS) with a formula of (CH$_3$)$_3$SiO-[(CH$_3$)$_2$SiO]$_n$-Si(CH$_3$)$_3$ [5]. The polymerisation degree, n, is calculated from the technical data sheet of the silicone manufacturer [5] to be 196. Because the crucible for silicone was kept in a glass tube at about 88 °C outside the alumina reactor [1], its equilibrium vapour pressure is expected to be high [6]. Vapour pressure of the silicone oil used in this study is not available and is assumed to be the same as that of (CH$_3$)$_3$SiO-[(CH$_3$)$_2$SiO]$_9$-Si(CH$_3$)$_3$ at 88 °C [6], $p_{silicone} = 2.8 \times 10^{-6}$ atm.

The silicone vapour species at 88 °C are unknown, and it is assumed here that no long chain polymer species survive at the reaction temperature of 650 °C. For simplicity, it is further assumed in what follows that the predominant species is the monomer, (CH$_3$)$_2$SiO.

Oxidation of silicone monomer is possible:

$$(CH_3)_2SiO(g) + 5H_2O(g) = SiO_2(s) + 2CO_2(g) + 8H_2(g) \tag{9}$$
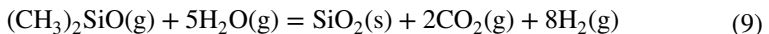
It is unlikely that reaction (9) might occur in the gas phase instead of at the sample surface for the following reasons. Firstly, the partial pressure $p_{silicone} = 2.8 \times 10^{-6}$ atm was small. The reactive gas species was not supersaturated nor was its partial pressure sufficiently high to form solid nuclei in the homogeneous gas phase. Secondly, the silicone gas was diluted markedly by the inert carrier Ar gas, reducing the probability of the molecular collisions needed for coalescence and growth of a nucleus. Finally any nuclei formed within the gas phase are likely to be carried

away by the flowing gas. Evidently the reaction is favoured at the oxide scale surface rather than in the gas phase. Factors contributing to this difference include the complexity of reaction (9) along with the dilute concentrations of reactants in the gas. These difficulties are overcome by adsorption on a suitable surface such as the scale. Specific catalytic processes on that surface may also accelerate reaction, but present results provide no information on this aspect.

It has been reported that SiO_2 formed by oxidation at 650 °C was amorphous [7] and solubility of SiO_2 in Cr_2O_3 is negligible [8]. On this basis, the detection by SAD of only crystalline Cr_2O_3 in the Si-rich outer scale layer (Figs. 3, 4) is explicable.

Chromia scales grow mainly by transport of Cr and oxygen species along grain boundaries [9, 10]. In the present case, formation of SiO_2 grains in the Si-rich outer scale layer reduced diffusion along Cr_2O_3 grain boundaries and consequently impeded grain growth. For this reason, Cr_2O_3 grains in the Si-rich outer layer were finer than those in the inner layer (Figs. 4, 5).

The Cr_2O_3 blades had different growth directions and their roots embedded to the underlying Cr_2O_3 scale (Figs. 2–4). As a result, small voids formed between the blade roots, providing a fast diffusion path into the scale for volatile Si species and extra nucleation sites for solid SiO_2 grains. Consequently, the outer Cr_2O_3 scale layer with the blades on top was rich in Si (Figs. 3, 4).

CVD of SiO_2 on Fe-30Cr

The Fe-30Cr alloy had a Cr concentration high enough to form a Cr_2O_3 scale. However, the (Cr, Si)-rich scale layers formed on Fe-30Cr and pure Cr in Ar-$10H_2O$-silicone had different morphologies and crystallinity: amorphous $(Cr,Si)O_x$ with Si-rich veins and random crystals on Fe-30Cr (Fig. 5), and a mixture of polycrystalline Cr_2O_3 and amorphous SiO_2 grains on pure Cr (Figs. 3, 4). The Si concentrations in the (Cr, Si)-rich scale layers were the same for Fe-30Cr and pure Cr (Figs. 4d, e, 5f), but a small Fe concentration (about 1.3 at.%) was always detected in the $(Cr,Si)O_x$ layer on Fe-30Cr (Fig. 5f). This difference implies that Fe-rich oxides might have an effect on the crystallinity of $(Cr,Si)O_x$.

At the initial reaction stage, oxides of Fe, Cr, and Si formed on the sample surface because of oxidation of Fe-30Cr and volatile Si species, forming an inner, polycrystalline Cr_2O_3 layer containing small amounts of Fe (2.4 at%) and Si (1.4 at.%) (layer 2, Fig. 5a, f). Transport of Fe species is kinetically and thermodynamically controlled. The thin, dense Cr_2O_3 layer acted as a barrier, reducing outward diffusion of Cr and Fe. The partial pressure of oxygen set by equilibrium of Cr_2O_3/Cr is too small to oxidise Fe at the scale-alloy interface and consequently no Fe oxides were incorporated into the Cr_2O_3 layer to diffuse outward. No visible pure Fe precipitates were observed in the amorphous $(Cr,Si)O_x$ layer (Fig. 5a, c). It is concluded that solid-state diffusion of Fe made a negligible contribution to the appearance of Fe in the outer, amorphous $(Cr,Si)O_x$ layer.

Volatile Fe species can be formed at the scale-alloy interface

$$Fe(s) + Cl_2(g) = FeCl_2(g) \quad \Delta G° = -184.2 \ (kJ) \ [4] \tag{10}$$
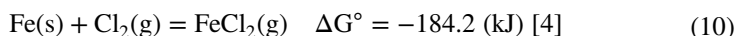
At the scale-gas interface where the oxygen partial pressure was high, oxidation of $FeCl_2$ formed iron oxides.

$$FeCl_2(g) + yH_2O(g) = FeO_y(s) + Cl_2(g) + yH_2(g) \tag{11}$$
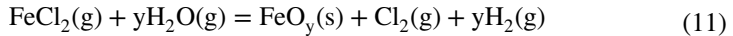
Thus a volatile iron chloride species is involved.

It seems that the formation of the amorphous $(Cr,Si)O_x$ phase (Fig. 5a) might need two factors: a gas mixture of siloxane-$CrCl_2$ and $FeCl_2$ catalyst. The available phase diagrams of Cr_2O_3-SiO_2 [8] and TiO_2-SiO_2 [11] show no intersolubility of the solid phases. However, an amorphous Ti-Si–O film can be formed by CVD [12]. As is now apparent, the same is true for Cr-Si–O.

Clearly, the amorphous Ti-Si–O and Cr-Si–O systems are not in an equilibrium state. In the current study, the amorphous $(Cr,Si)O_x$ formed on Fe-30Cr but not pure Cr. It is suggested that the simultaneous presence of gaseous Fe, Cr and Si compounds led to deposition on a very fine scale, resulting in the formation of amorphous $(Cr,Si)O_x$ material. This amorphous phase was only marginally stable at 650 °C, as evidenced by precipitation of fine crystalline grains within the $(Cr,Si)O_x$ layer (Fig. 5a).

Within the amorphous material, Si-rich oxide veins aligned in the growth direction separated the surrounding, columnar $(Cr,Si)O_x$ cells (Fig. 5a, b). Interfaces between the Si-rich veins and $(Cr,Si)O_x$ cells might contribute to diffusion during scale growth. Further study is necessary to understand transport of species through the amorphous $(Cr,Si)O_x$ layer. The formation of amorphous $(Cr,Si)O_x$ is summarised schematically in Fig. 11. At the scale-alloy interface, volatile $CrCl_2$ and $FeCl_2$ species formed by reactions (2, 5, 10) and solid Cr_2O_3 by reaction (1). At the scale-gas interface, these volatile chloride species were mixed with silicone vapour and oxidised to form $(Cr,Si)O_x$ by reactions (4, 9, 11).

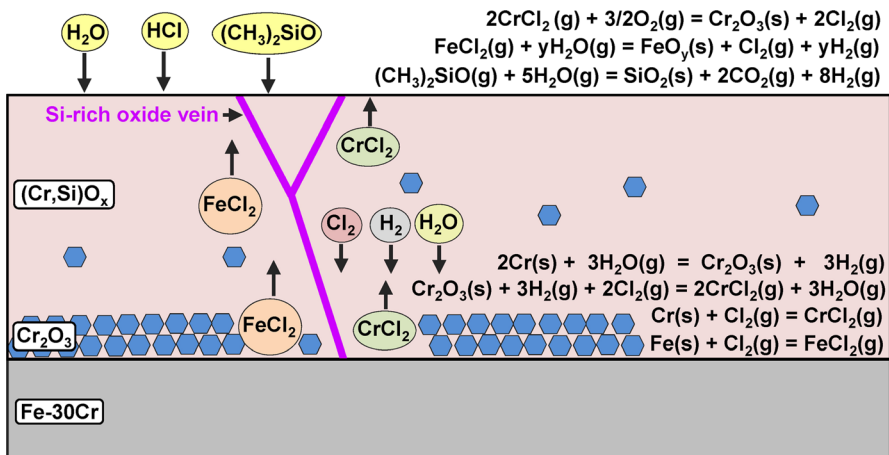**Fig. 11** Proposed mechanism of amorphous $(Cr,Si)O_x$ formation on Fe-30Cr

Both materials formed inner layers of crystalline Cr_2O_3, but in both cases it was porous, probably not contributing much to overall rate control. The difference arises in the outer dense material: crystalline chromia plus amorphous silica in the pure Cr case, but glassy mixed oxide in the alloy case. Given the different microstructures and phase constitutions of the two scales, it is not surprising that the kinetics and growth rates differ.

CVD of SiO_2 on Kanthal Alloy

Oxidation of Kanthal alloy in dry O_2 at 600–700 °C results in an Al_2O_3 scale containing Fe and Cr (less than 10 at. %) [13]. In the present work, Kanthal formed three different Si-rich corrosion products on the surface: amorphous $(Cr,Si)O_x$ nodules on $(Cr,Fe)_{23}C_6$ precipitates (Fig. 7a), a duplex scale of (Si, Fe)-rich and (Al, Cr)-rich layers (Fig. 8), and a duplex scale of Si-rich and (Al, Cr)-rich layers (Fig. 9). The formation of the amorphous $(Cr,Si)O_x$ nodules is now considered.

The experimental result (Fig. 7) and Thermocalc phase diagram (Fig. 10) confirmed that the alloy carbon concentration was sufficient to form (Cr,Fe)-rich carbide precipitates in the alloy. The Thermocalc software [3] predicted a carbide volume fraction of 0.5%. Assuming the $(Cr,Si)O_x$ nodules cover whole carbide precipitates, the measured nodule area fraction of 0.4% corresponds well with the value 0.5% predicted by Thermocalc. The 0.1% difference between the measured and predicted volume fractions is due to other high Al content carbides which did not form $(Cr,Si)O_x$ nodules. The amorphous $(Cr,Si)O_x$ nodules formed on the carbide precipitates containing a very low Al concentration, with insignificant EDX spectrum peaks of Al (Fig. 7c). Other carbide precipitates with a higher Al concentration were able to form and maintain a thin, Al-rich scale (Figs. 8e). The $(Cr,Si)O_x$ formation consumed Cr in the underlying carbide, enriching Fe and Al in the underlying carbide (Fig. 7f, g). Therefore, an Al_2O_3 layer can form at the nodule-carbide interface (Fig. 7f, g, h, k). The formation of $(Cr,Si)O_x$ nodules on top of the Si-free carbide precipitates also confirms that the Si supply for the nodule growth was volatile Si species in the reaction gas.

The amorphous $(Cr,Si)O_x$ nodules formed only on Cr-rich oxide scales. For this reason, this amorphous $(Cr,Si)O_x$ phase was observed above the (Cr,Fe)-rich carbide precipitates but not on other Al-rich regions, which formed an Al-rich oxide scale.

The thin scale on Kanthal alloy consisted of an outer Si-rich layer and an inner (Al, Cr)-rich layer (Figs. 8, 9). The Si concentration in the outer layer was up to 31.8 at.% (Fig. 8a, c). The equilibrium oxygen partial pressures (p_{O_2}) of Al_2O_3, SiO_2, and Cr_2O_3 calculated using activity of Al and Cr in the alloy ($a_{Al} = 0.11$, $a_{Cr} = 0.22$) and $a_{Si} = 1$ at 650 °C are 3.2×10^{-51}, 4.1×10^{-43}, and 4×10^{-33} atm, respectively. The p_{O_2} value of the reaction gas at 650 °C is 4.5×10^{-9} atm. It is clear that the inner (Al, Cr)-rich layer can continue to grow beneath the Si-rich outer layer by oxidation of only Al. The presence of less stable Fe and Cr oxides in the outer Si-rich layer and the inner Al-rich layer is due to initial stage oxidation.

The solubility of Cr_2O_3 in Al_2O_3 is limited for a ratio of $Cr_2O_3/(Cr_2O_3 + Al_2O_3)$ (mol %) from 2.5 to 72.5 at 650 °C and 1 atm [14]. Therefore, the inner (Al, Cr)-rich

layer (Figs. 8, 9) were mainly made up of a mixture of two crystalline phases of Al_2O_3-rich and Cr_2O_3-rich solid solutions.

The exposure of Kanthal alloy to Ar-10H$_2$O-0.1HCl-silicone oil can, at least in principle, result in vaporisation of Al at the scale-alloy interface.

$$Al(s) + 3/2Cl_2(g) = AlCl_3(g) \quad \Delta G° = -538.2 \text{ (kJ) [4]} \tag{12}$$

The inner (Al, Cr)-rich layer on Kanthal alloy grew slower than the Cr-rich scales on pure Cr and Fe-30Cr, leading to the smallest weight uptake for Kanthal alloy (Fig. 1). It is clear that the inner (Al, Cr)-rich layer was an effective diffusion barrier. The duplex scale on Kanthal alloy consisted of slow-growing, dense Si-rich and (Al, Cr)-rich layers. On this basis, it is likely that inward transport of Cl$_2$ species through the scale on Kanthal alloy was impeded significantly, and therefore the formation of volatile AlCl$_3$ from the reaction (8) was negligible.

Mass Transfer of Si

The formation of Si-rich oxide layers on pure Cr (up to 9.5 at.% Si, Fig. 4), Fe-30Cr (8.3 at.% Si, Fig. 5), and Kanthal (up to 31.8 at.% Si, Fig. 8) confirms the chemical vapour deposition of SiO$_2$ during the exposure to Ar-10H$_2$O-0.1HCl-silicone oil at 650 °C. Clearly, the partial pressure of volatile Si species in the reaction gas was sufficient for the CVD of SiO$_2$.

Assuming the whole duplex chromia scales on either pure Cr or Fe-30Cr had the same Si concentration of the Si-rich outer scale layer, the total amount of Si in the Cr$_2$O$_3$ scales after 240 h reactions is

$$n_{Si}^{scale} = \frac{N_{Si}}{N_{Cr}} n_{Cr}^{scale} \tag{13}$$

where N_{Si} and N_{Cr} are average concentrations (atom %) of Si and Cr in the (Cr, Si)-rich layer measured by TEM/EDX analysis (Figs. 4, 5), and n_i^{scale} the amount of indicated component per unit surface area in the scale (mol/cm^2). Values of (N_{Si}, N_{Cr}) (at. %) are (7.1, 34.2) for pure Cr and (10.2, 33.6) for Fe-30Cr.

Approximating the scale formed on Fe-30Cr as pure Cr$_2$O$_3$

$$n_{Cr}^{scale} = 2\frac{\delta_{scale}\rho_{Cr_2O_3}}{M_{Cr_2O_3}} \tag{14}$$

where $\rho_{Cr_2O_3}$ and $M_{Cr_2O_3}$ are density and molar mass of Cr$_2$O$_3$, and average scale thickness $\delta_{scale} = 355$ nm (pure Cr) and 380 nm (Fe-30Cr). The Si amount deposited onto Cr$_2$O$_3$ blades on pure Cr (Fig. 2b) was neglected in the calculation. Sample surface areas (A) were 2.3 cm^2 (pure Cr) and 1.6 cm^2 (Fe-30Cr), yielding n_{Si}^{scale} values of 5×10^{-7} mol/cm^2 or 1.2×10^{-6} mol for pure Cr, and 7.9×10^{-7} mol/cm^2 or 1.3×10^{-6} mol for Fe-30Cr.

The Si-rich outer scale layer on Kanthal alloy had a variable thickness (15–50 nm) and Si concentration (8.1–31.8 at.%) (Figs. 8, 9). Assuming the Si-rich outer scale

layer is SiO_2 and $\delta_{SiO_2} = 50$ nm thick, the total maximum amount of Si in the scale after 240 h reactions is

$$n_{Si}^{scale} = \frac{\delta_{SiO_2} \rho_{SiO_2}}{M_{SiO_2}} \tag{15}$$

where ρ_{SiO_2} and M_{SiO_2} are density and molar mass of SiO_2, yielding $n_{Si}^{scale} = 2.2 \times 10^{-7}$ mol/cm^2 or 3.1×10^{-7} mol for a surface area of 1.4 cm^2.

The weight loss of silicone oil in the crucible after the 240 h reaction was 6.2 mg, yielding the amount of Si vaporised from the silicone oil crucible of $n_{Si}^{silicone\ crucible} = 8.4 \times 10^{-5}$ mol. Clearly, the amount of silicone vapour in the reaction gas was sufficient to account for the silicon oxides incorporated into the Cr_2O_3 and Al-rich scales growing on pure Cr/Fe-30Cr and Kanthal.

Conclusions

Chemical vapour deposition of SiO_2 during corrosion in Ar-10H$_2$O-0.1HCl at atmospheric pressure was achieved using silicone vapour formed by heating silicone oil at low temperature.

Pure Cr formed a crystalline Cr_2O_3 scale containing amorphous SiO_2. It is suggested that porous Cr_2O_3 blades on top of the scale were formed by oxidation of volatile Cr chlorides.

The Fe-30Cr alloy formed a scale consisting of an amorphous $(Cr,Si)O_x$ layer and a thin polycrystalline Cr_2O_3 layer underneath. The amorphous $(Cr,Si)O_x$ contained a small Fe concentration of about 1.3 at.%. and was at non-equilibrium state. It is suggested that the formation of amorphous $(Cr,Si)O_x$ becomes possible because of oxidation of a gas mixture of (Cr, Si) species and $FeCl_2$. The amorphous oxide coating is not formed in the absence of iron, its presence and that of HCl are essential. It is concluded on this basis that $FeCl_2$ (g) is required for the CVD process to succeed.

Kanthal alloy contained a small carbon concentration, leading to the formation of internal $(Cr,Fe)_{23}C_6$ precipitates after the reactions at high temperature. The amorphous $(Cr,Si)O_x$ compound formed on top of the $(Cr,Fe)_{23}C_6$ precipitates, whereas the other sample regions were covered by a thin, duplex scale of an outer Si-rich layer and an inner Al-rich layer.

Author contributions Thuan Dinh Nguyen: Methodology, Formal analysis, Investigation, Writing - Original draft, Visualization. Jianqiang Zhang: Supervision, Methodology, Validation, Writing-Review & editing, Funding acquisition, Project administration. David J. Young: Supervision, Methodology, Validation, Writing-Review & editing, Funding acquisition, Project administration.

Declarations

References

1. T. D. Nguyen, J. Zhang, and D. J. Young, *Corrosion Science* **209**, 110808 (2022).
2. R. H. Perry, D. W. Green, and J. O. Maloney, *Perry's Chemical Engineers' Handbook*, 7th edn. (McGraw-Hill, 1997).
3. Thermocalc 2021b. Database: TCFE11.
4. FactSage 8.1. Database: FactPS.
5. https://www.silitech.ch/wp-content/uploads/2021/03/32.pdf
6. D. F. Wilcock, *Journal of the American Chemical Society* **68**, 691–696 (1946).
7. T. D. Nguyen, J. Zhang, and D. J. Young, *Oxidation of Metals* **87**, 541–573 (2017).
8. E. N. Bunting, *Journal of Research of the National Bureau of Standards* **5**, 325–327 (1930).
9. D. Caplan and G. I. Sproule, *Oxidations of Metals* **9**, 459–472 (1975).
10. R. J. Hussey, D. F. Mitchell, and M. J. Graham, *Materials and Corrosion* **38**, 575–583 (1987).
11. E. N. Bunting, *Journal of Research of the National Bureau of Standards* **11**, 719–725 (1933).
12. A. Hodroj, J. L. Deschanvres, and U. Gottlieb, *Journal of The Electrochemical Society* **155**, D110–D114 (2008).
13. H. Josefsson, F. Liu, J.-E. Svensson, M. Halvarsson, and L.-G. Johansson, *Materials and Corrosion* **56**, 801–805 (2005).
14. W. Sitte, *Materials Science Monographs* **28A**, 451–456 (1985).